ChemComm

Accepted Manuscript

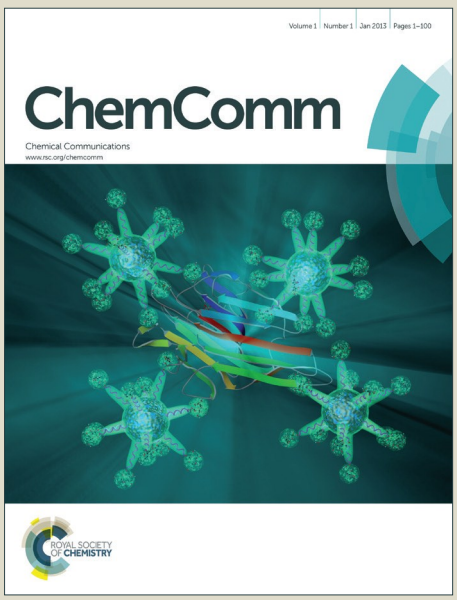

ROYAL SOCIETY OF CHEMISTRY

www.rsc.org/chemcomm

Journal Name

RSCPublishing

COMMUNICATION

Bismuth oxyiodide nanosheets: a novel high-energy anode material for lithium-ion batteries

Cite this: DOI: 10.1039/xoxxoooooox

Chaoji Chen,‡ Pei Hu,‡ Xianluo Hu,* Yueni Mei and Yunhui Huang*

Received ooth January 2012,
Accepted ooth January 2012

DOI: 10.1039/xoxxoooooox

www.rsc.org/chemcomm

BiOI nanosheets are easily synthesized by direct thermal treatment of commercial BiI_3 powder, serving as a novel anode material for lithium-ion batteries. A high volumetric capacity of ~5678 mA h cm^{-3} was achieved. This work demonstrates that the BiOI nanosheets hold great promise as high-energy anode materials for lithium-ion batteries.

Lithium-ion batteries (LIBs) have recently gained intensive attention and have been widely used in mobile devices and electric vehicles.[1–3] Current LIBs are mainly built on intercalation chemistry that involves Li-ion insertion/exaction in the crystal lattice, such as $LiFePO_4$ cathodes and TiO_2 anodes.[4–6] The electrodes based on an intercalation reaction often involve small volume expansion and high stability of the crystal structure. Consequently, good rate capability and cyclability can be achieved. Nevertheless, Li-ion storage based on intercalation chemistry is often limited (e.g., generally 1 or less per unit cell), resulting in a relatively low energy density. Electrode materials (e.g., SnO_2 and Si) containing group IVA or VA elements can store Li^+ ions through electrochemical alloy/dealloy reactions.[7–10] For example, Si could electrochemically react with 4.4 Li per unit cell, thereby yielding a high gravimetric and volumetric theoretical capacity.[9–10] Based on the Bi^+/Bi^{3+} redox couple and the electrochemical activity between Bi and Li, Bi-based materials are novel candidates as anodes for LIBs. Despite the relatively low theoretical gravimetric capacity (386 mA h g^{-1}), bismuth can deliver a high volumetric capacity of ~3765 mA h cm^{-3}, which is promising for LIBs with high energy densities.

Here we report for the first time on Li^+-storage properties of layer-structured BiOI nanosheets that are easily prepared by direct thermal treatment of commercial BiI_3 powder in air. The Li-cycling mechanism was explored in detail by ex-situ X-ray diffraction (XRD), Raman spectroscopy, and X-ray photoelectron spectroscopy (XPS), which have been proved to be powerful in investigating the lithiation/delithiation processes in a wide range of electrode materials.[11-15] Our results show that an alloy-based mechanism dominates the electrochemical Li-cycling process in the layered BiOI anode material.

Briefly, commercial BiI_3 powder was annealed in air at an optimized temperature of 300 ˚C for 8 h. After removal of residual I_2 with ethanol and DI water, BiOI nanosheets were obtained. Fig. 1a shows the powder XRD pattern of the BiOI product. All the peaks can be indexed to a tetragonal phase of BiOI (JCPDF no. 10-0445). The morphology and microstructure of the BiOI product were investigated by scanning electron microscopy (SEM) and transmission electron microscopy (TEM). The SEM and TEM images of Fig. 1b and 1c indicate that the nanosheets are several micrometers in size and a few tens of nanometers in thickness. The high-magnification TEM image (Fig. 1d) reveals that numerous nanopores exist in the BiOI nanosheet. The clear lattices with spacings of 0.28 nm were observed in the high-resolution TEM image (Fig. S1), which agrees well with the XRD result.

The lithium-storage performances of the as-formed BiOI

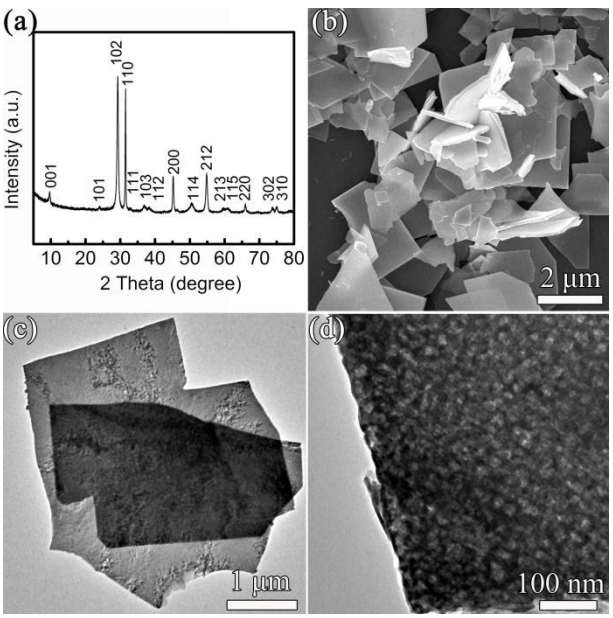

Fig. 1 (a) XRD pattern, (b) SEM image, (c, d) TEM images of the BiOI product.

nanosheets were investigated in detail by half coin cells using active materials as the working electrode and a lithium foil as the counter electrode. The coin cells were disassembled at different discharge-charge status to explore the detailed electrochemical reactions by XRD analyses (Fig. 2). During the lithiation process, a distinct plateau appears at ~1.65 V. Ex-situ XRD patterns suggest that the crystal phase of BiOI in the fresh electrode transformed into metallic Bi during the state of 0→1. Upon discharge to 1 V (2), the enhanced XRD peaks for metallic Bi indicates the transformation was nearly complete. As the lithiation process proceeded, two plateaus started to emerge at ~0.75 (2→3) and ~0.7 V (3→4), respectively, which are related to the alloying process of metallic Bi with lithium.[16] The corresponding XRD pattern for (4) confirms that Li_3Bi was formed when discharged to ~0.6 V. As the voltage further decreased to the end of discharge at 0.05 V (4→6), there appeared a slope region that is assigned to the formation of a surface electrolyte interface (SEI) layer and interfacial lithium storage.[17] During the charge process, there is a long plateau region at ~0.9 V, which is attributed to the dealloy process of Li_3Bi. The ex-situ XRD analyses reveal that the peaks for Li_3Bi disappeared when charged to 2.6 V (10), but metallic Bi was generated.

Although the ex-situ XRD analyses could provide the important information on the evolution of crystal phases during the first discharge-charge process, the details on the amorphous products were hardly obtained. It is known that Raman spectroscopy and XPS are proven to be powerful techniques for studying oxidation states of both crystalline and amorphous phases. The BiOI electrodes that were disassembled at various discharge status during the first cycle has been explored by ex-situ Raman spectroscopy (Fig. S2). Upon Li-insertion, the signals for Bi–Bi vibrations (~80 and ~255 cm^{-1}) increased evidently, while the signals for Bi–O vibrations at ~125 cm^{-1} were weakened. This also confirms that the conversion of BiOI into metallic Bi during the lithiation process, which agrees well with the XRD results. Meanwhile, the peaks at ~500 and ~620 cm^{-1} were found to be absent, due the decomposition of BiOI.

Fig. 3 shows the ex-situ XPS results for electrochemical reactions. Clearly, the peaks for Bi 4f in the high-resolution XPS spectra were shifted to the higher energy, in contrast to the fresh electrode. This suggests that a conversion from Bi–O to Bi–Bi or Bi–Li interactions occurred upon Li-ion lithiation and extraction. Interestingly, the peaks of I 3d in the survey XPS spectra disappeared upon lithiation (Fig. S3), suggesting that soluble LiI may be generated. It is noted that the evolution for O 1s is obvious (Fig. 3c). When the voltage continued to decrease during the discharge process, the peaks for Bi–O bonds disappeared, arising from the decomposition of BiOI. This transformation process was also accompanied by the formation of Li-containing oxides or carbonates, such as Li_2O and Li_2CO_3, because of the presence of O–Li bonds during the discharge process. During the subsequent charge process, the slightly enhanced peaks for Bi–O are attributed to the partly conversion of Li_2O to Bi_2O_3 ($3Li_2O + 2Bi \leftrightarrow Bi_2O_3 + 6Li$).[16] The electrodes upon Li lithiation/extraction were further investigated by TEM. Fig. S4 displays the TEM images for the product obtained at the discharge state of 0.05 V. It is observed that a large numbers of tiny nanocrystals are distributed on an amorphous matrix (Fig. S4a). Each nanocrystal has distinct lattice spacing of 0.33 nm corresponding to (012) planes of Bi, which is consistent well with the XRD and Raman results.

Based on the above ex-situ analyses, the electrochemical reactions are schematically summarized in Scheme 1. The electrochemical discharge process starts with the decomposition of BiOI, and metallic Bi, Li_2O and LiI are generated. Note that LiI may be soluble in the carbonate-based electrolyte, and thus it would not participate in the subsequent electrochemical process. Besides, amorphous Li_2O would act as a matrix for the subsequent alloy/dealloy reactions between metallic Bi and lithium. Upon discharge to below ~1 V, the alloy process of Bi takes place. It begins with the formation of alloy (or solid solution) with low Li content, in the form of LiBi. As the voltage continues to decrease, more Li would alloy with Bi, leading to the formation of Li_3Bi alloy, or solid solution with 3 Li per Bi. At the end of the discharge process, interfacial lithium absorption and the SEI layer contribute to the additional capacity assigned to the slope region at the tail of the discharge profile.[17] Generally, the formation of the SEI film occurs below 1 V. However, it also possibly starts above 1 V due to the formation of LiF.[18] In the subsequent charging and discharging processes, reversible dealloy/alloy reactions between Bi and Li will dominate the electrochemical lithium storage, together with a minor contribution from the reversible reaction of $3 Li_2O + 2 Bi \leftrightarrow Bi_2O_3 + 6 Li$.[16]

As a new anode material for LIBs, the electrochemical performance of this material should be important for use in the practical case. In this regard, we further explored the electrochemical

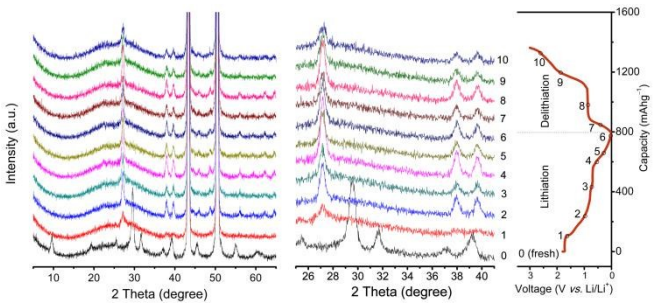

Fig. 2 Ex-situ XRD patterns of the BiOI electrode and the corresponding charge-discharge profiles at 15 mA g^{-1} for the first cycle. The two strong peaks at 43.5˚ and 50.5˚ arise from the Cu foil current collector.

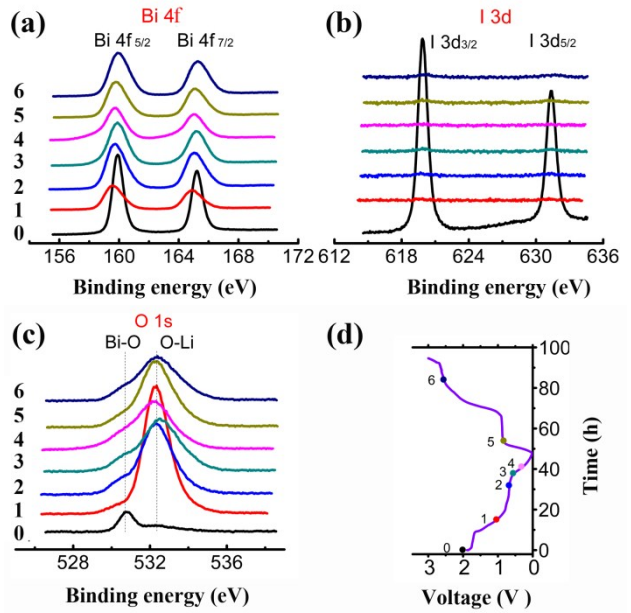

Fig. 3 Ex-situ high-resolution XPS spectra of the BiOI electrode: a) Bi 4f, b) I 3d, c) O 1s; d) The corresponding charge-discharge profiles at 30 mA g^{-1}.

performance of the layered BiOI nanosheets. As shown in Fig. 4a, the CV curve in the initial cycle shows three reduction peaks at ~1.65, 0.75 and ~0.7 V, assigned to the conversion of BiOI to metallic Bi, the formation of LiBi and Li_3Bi alloy (or solid solution), respectively. The strong oxidation peak at ~0.9 V is associated with the dealloy process. It is not surprising that the reduction peak at ~1.65 V disappeared in the second and the subsequent cycles, while the other two were kept, indicating the reversibility of the alloy/dealloy reactions after the first cycle. The charge-discharge profiles of the initial 7 (or 6) cycles were collected within two different potential windows: 3.0–0.05 V and 2.5–0.5 V at a current density of 30 mA g^{-1}. A high initial discharge capacity of ~717 mA h g^{-1} was obtained at a wider potential window. Note that a much higher volumetric capacity of ~5678 mA h cm^{-3} was delivered, considering the high density of BiOI (7.922 g cm^{-3}). Similar to the other anode materials based on an alloy/dealloy mechanism, obvious decay in capacity upon cycling was observed, which is mainly attributed to the volume expansion during lithiation.[7–10] Rational carbon coating, fabricating unique nanostructures or carbon hybridization are proven to be effective strategies for enhancing the cyclability of this kind of anode materials.[7,10,19] If a narrower potential window of 2.5–0.5 V was selected, better cyclability was achieved despite the slight decrease in capacity in the initial cycles (Fig. 4b). This may be attributed to the reduced side reactions between the electrode and the electrolyte. For comparison, the charge-discharge profiles within the two potential windows are shown in Fig. 4c and 4d. The BiOI electrode exhibits a high specific gravimetric capacity, especially a high volumetric capacity of ~5678 mA h cm^{-3} within a potential window of 3–0.05 V, and enhanced cyclability within a narrower and safer potential window (2.5–0.5 V).

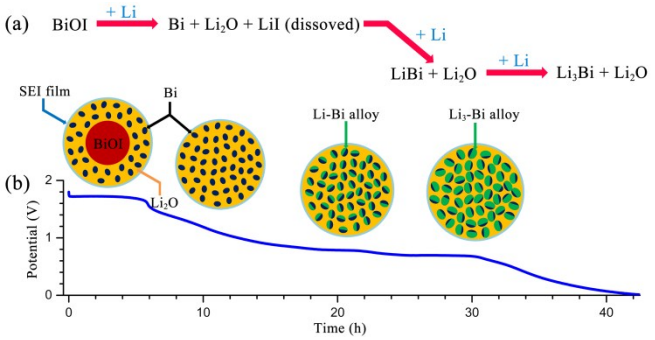

Scheme 1 (a) Overall reaction pathway in the BiOI-Li cell during the discharge process in the first cycle. (b) The initial discharge profile of the BiOI-Li cell and the schematic illustrations of phase evolution upon discharging.

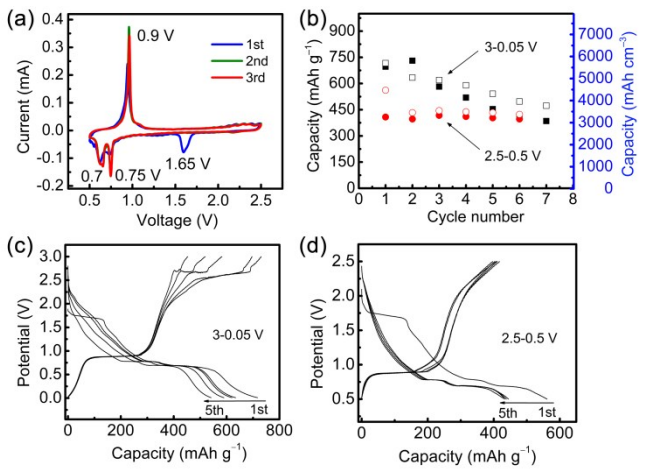

Fig. 4 (a) Electrochemical performance of the BiOI electrode: (a) CV curves in a voltage range of 0.5–2.5 V at 0.2 mV s^{-1}, (b) cycle performances at 30 mA g^{-1} with different charge-discharge voltage windows, (c,d) discharge-charge profiles in a voltage range of 3–0.05 V and 2.5–0.5 V, respectively.

In conclusion, a new anode material of layered BiOI with a high volumetric capacity is developed for the first time, whereby it was easily prepared by direct thermal treatment of commercial BiI_3 powder in air. Ex-situ XRD, Raman spectroscopy and XPS have been utilized to systematically analyze the electrochemical processes. The unique electrode made of BiOI nanosheets exhibits a high volumetric capacity of ~5678 mA h cm^{-3}. The present method is facile, and promising for large-scale industrial production. After surface modification with carbon, the electrode material may find useful applications in LIBs with high energy densities.

This work was supported by the Natural Science Foundation of China (no. 21271078 and 51472098), Program for New Century Excellent Talents in University (no. NECT-12-0223), and Program for Changjiang Scholars and Innovative Research Team in University (no. IRT1014).

Notes and references

State Key Laboratory of Materials Processing and Die & Mould Technology, School of Materials Science and Engineering, Huazhong University of Science and Technology, Wuhan 430074, P. R. China.
E-mail: huxl@mail.hust.edu.cn; huangyh@mail.hust.edu.cn
‡ *These authors contributed equally to this work*

Electronic Supplementary Information (ESI) available: Experimental details, Raman spectra and TEM images. See DOI: 10.1039/c000000x/

1. A. S. Arico, P. Bruce, B. Scrosati, J. M. Tarascon and W. Van Schalkwijk, *Nat. Mater.*, 2005, **4**, 366–377.
2. P. G. Bruce, B. Scrosati and J. M. Tarascon, *Angew. Chem. Int. Ed.*, 2008, **47**, 2930–2946.
3. J. B. Goodenough and K. S. Park, *J. Am. Chem. Soc.*, 2013, **135**, 1167–1176.
4. L. L. Peng, Y. Zhao, Y. Ding and G. H. Yu, *Chem. Commun.*, 2014, **50**, 9569–9572.
5. C. J. Chen, X. L. Hu, Z. H. Wang, X. Q. Xiong, P. Hu, Y. Liu and Y. H. Huang, *Carbon*, 2014, **69**, 302–310.
6. C. J. Chen, X. L. Hu, Y. Jiang, Z. Yang, P. Hu and Y. H. Huang, *Chem. Eur. J.*, 2014, **20**, 1383–1388.
7. L. Zhang, H. B. Wu, B. Liu and X. W. Lou, *Energy Environ. Sci.*, 2014, **7**, 1013–1017.
8. V. Aravindan, K. B. Jinesh, R. R. Prabhakar, V. S. Kale and S. Madhavi, *Nano Energy*, 2013, **2**, 720–725.
9. X. Su, Q. L. Wu, J. C. Li, X. C. Xiao, A. Lott, W. Q. Lu, B. W. Sheldon and J. Wu, *Adv. Energy Mater.*, 2014, **4**, 1300882.
10. N. Liu, Z. D. Lu, J. Zhao, M. T. McDowell, H.-W. Lee, W. T. Zhao and Y. Cui, *Nat. Nanotech.*, 2014, **9**, 187–192.
11. C.-M. Park, S. Yoon, S.-I. Lee and H.-J. Sohn, *J. Power Sources*, 2009, **186**, 206–210.
12. M. A. Reddy and U. Varadaraju, *J. Electrochem. Soc.*, 2014, **161**, A149–A153.

13. S. Brutti, V. Gentili, H. Menard, B. Scrosati and P. G. Bruce, *Adv. Energy Mater.*, 2012, **2**, 322–327.
14. J. J. Saavedra-Arias, N. K. Karan, D. K. Pradhan, A. Kumar, S. Nieto, R. Thomas and R. S. Katiyar, *J. Power Sources*, 2008, **183**, 761–765.
15. S.-W. Kim, H.-W. Lee, P. Muralidharan, D.-H. Seo, W.-S. Yoon, D. K. Kim and K. Kang, *Nano Res.*, 2011, **4**, 505–510.
16. Y. L. Li, M. A. Trujillo, E. G. Fu, B. Patterson, L. Fei, Y. Xu, S. G. Deng, S. Smirnov and H. M. Luo, *J. Mater. Chem. A*, 2013, **1**, 12123–12127.
17. J. Y. Shin, D. Samuelis and J. Maier, *Adv. Funct. Mater.*, 2011, **21**, 3464–3472.
18. Y. Y. Hu, Z. Liu, K. W. Nam, O. J. Borkiewicz, J. Cheng, X. Hua, M. T. Dunstan, X. Yu, K. M. Wiaderek, L. S. Du, K. W. Chapman, P. J. Chupas, X. Q. Yang and C. P. Grey, *Nat. Mater.*, 2013, **12**, 1130–1136.
19. S. Yang, W. B. Yue, J. Zhu, Y. Ren and X. J. Yang, *Adv. Funct. Mater.*, 2013, **23**, 3570–3576.